A novel gene-screening approach reveals QSOX1/IL1RAP as promising biomarkers for the severity of non-alcoholic fatty liver disease

Wenfeng Ma [1,2,3,4], Jinrong Huang [2], Benqiang Cai [1,4], Mumin Shao [6,7], Xuewen Yu [6,7], Mikkel Breinholt Kjær [5,8], Minling Lv [1,4], Xin Zhong [1,4], Shaomin Xu [1,4], Bolin Zhan [1,4], Qun Li [1,4], Qi Huang [1,4], Mengqing Ma [1,4], Lei Cheng [2], Yonglun Luo [2,3]*, Henning Grønbæk [5]*, Xiaozhou Zhou [1,4]*, Lin Lin [2,3]*

1 Department of Liver Disease, Shenzhen Traditional Chinese Medicine Hospital, Shenzhen, Guangdong 518033, China.

2 Department of Biomedicine, Aarhus University, Aarhus, Denmark.

3 Steno Diabetes Center Aarhus, Aarhus University Hospital, Aarhus, Denmark.

4 Department of Liver Disease, The Fourth Clinical Medical College of Guangzhou University of Chinese Medicine, Shenzhen, 518033, China.

5 Department of Hepatology and Gastroenterology, Aarhus University Hospital, Aarhus, Denmark.

6 Department of Pathology, Shenzhen Traditional Chinese Medicine Hospital, Shenzhen, Guangdong 518033, China.

7 Department of Pathology, The Fourth Clinical Medical College of Guangzhou University of Chinese Medicine, Shenzhen, 518033, China.

8 Department of Clinical Medicine, Aarhus University, Aarhus, Denmark.

* = corresponding author

Highlights

RNA-seq data from 625 liver specimens comprising healthy controls and NAFLD

patients with increasing severity were utilized for screening NAFLD biomarkers.

- A novel unsupervised method for clustering genes based on the similarity of gene expression across each sample enhanced the discovery of novel effective non-invasive NAFLD biomarkers.
- QSOX1, IL1RAP, and especially the QSOX1/IL1RAP ratio, were found to be associated with NAFLD severity.
- The high sensitivity of the QSOX1/IL1RAP ratio in predicting NAFLD severity was validated with plasma proteomics quantification (AUROC = 0.95) and ELISA (AUROC = 0.82) in two independent patient cohorts.

Abstract

Background and Aims: Non-alcoholic fatty liver disease (NAFLD) is a progressive liver disease that ranges from simple steatosis to inflammation, fibrosis, and cirrhosis. To address the unmet need for new NAFLD biomarkers, we aimed to identify candidate biomarkers using publicly available RNA sequencing (RNA-seq) and proteomics data.

Methods: A novel approach involving unsupervised gene clustering was performed using homogeneously processed and integrated RNA-seq data of 625 liver specimens to screen for NAFLD biomarkers in combination with public proteomics data from healthy controls and NAFLD patients. Additionally, we validated the results in the NAFLD and healthy cohorts using enzyme-linked immunosorbent assay (ELISA) of plasma and immunohistochemical staining (IHC) of liver samples.

Results: We generated a database (https://dreamapp.biomed.au.dk/NAFLD/) for exploring gene expression changes along NAFLD progression to facilitate the identification of genes and pathways involved in the disease's progression. Through cross-analysis of the gene and protein clusters, we identified 38 genes as potential biomarkers for NAFLD severity. Up-regulation of Quiescin sulfhydryl oxidase 1

(*QSOX1*) and down-regulation of Interleukin-1 receptor accessory protein (*IL1RAP*) were associated with increasing NAFLD severity in RNA-seq and proteomics data. Remarkably, the QSOX1/IL1RAP ratio in plasma demonstrated effectiveness in diagnosing NAFLD, with an area under the receiver operating characteristic (AUROC) of up to 0.95 as quantified by proteomics profiling and an AUROC of 0.82 with ELISA. **Conclusions:** We discovered a significant association between the levels of QSOX1/IL1RAP and NAFLD severity. Furthermore, the QSOX1/IL1RAP ratio shows promise as a non-invasive biomarker for diagnosing NAFLD and assessing its severity. (ChiCTR2300073940).

Lay Summary

This study aimed to find non-invasive biomarkers for non-alcoholic fatty liver disease (NAFLD). Researchers utilized a new gene clustering method to analyze RNA-seq data from 625 liver samples. The identified biomarkers were further validated using plasma proteomics profiling, enzyme-linked immunosorbent assay (ELISA), and liver immunohistochemical staining (IHC) in three separate groups of healthy controls and NAFLD patients. The study revealed that the levels of QSOX1 were elevated while IL1RAP levels were reduced with increasing severity of NAFLD. Notably, the ratio of QSOX1 to IL1RAP expression in plasma showed promise as a non-invasive diagnostic tool for assessing the severity of NAFLD, eliminating the reliance on liver biopsy.

Graphical abstract

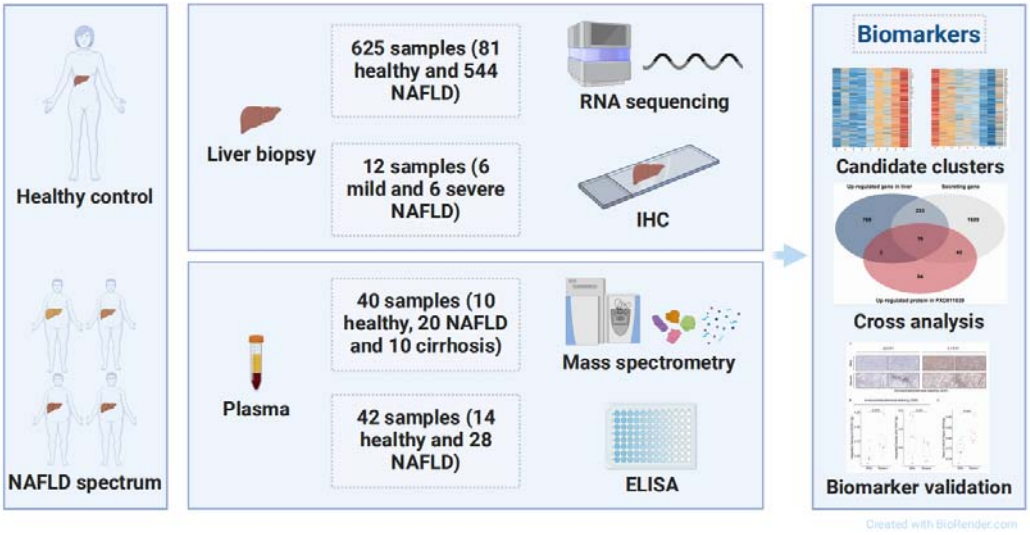

Keywords

Non-alcoholic fatty liver disease, RNA sequencing data integration, non-invasive biomarker, quiescin sulfhydryl oxidase 1, interleukin-1 receptor accessory protein

Introduction

Non-alcoholic fatty liver disease (NAFLD) is an acknowledged hepatic manifestation of the metabolic syndrome, with an estimated global prevalence of around 25-32% (1, 2). The severity of this liver disease ranges from Non-alcoholic Fatty Liver (NAFL) with simple steatosis to Non-alcoholic Steatohepatitis (NASH) with inflammation and fibrosis, which can progress to NASH-induced cirrhosis and increase the risk of hepatocellular carcinoma (HCC).

The gold standard for diagnosing NAFLD is still liver biopsy histologically, despite its associated side effects such as pain, bleeding, and rare mortality. The need for novel, precise, cost-effective imaging tools and non-invasive biomarkers is still unmet to address these drawbacks and reduce costs (3). Moreover, non-invasive biomarkers are highly needed for replacing repeated liver biopsies when assessing liver histology during pharmacological interventions. Existing NAFLD biomarkers primarily focus on steatosis (e.g., SteatoTest™ or the lipid accumulation product), inflammation (e.g., circulating keratin 18 fragments [CK18), soluble CD163) or fibrosis (e.g., ELF, FibroTest or Pro-C3 tests) (4-8). Despite advancements in biomarker technology, development, and evaluation, an ideal biomarker for the diagnosis, prognosis, and assessment of treatment effects in NAFLD has yet to be identified.

In recent years, advancements in technologies such as RNA sequencing (RNA-seq), single-cell analysis, and spatial transcriptomics have provided deeper insights into the molecular and cellular processes involved in NAFLD progression (9-11). Large-scale profiling efforts, combined with targeted validation approaches, have led to the discovery of potential biomarkers (12, 13). However, the majority of available RNA-seq data are derived from smaller cohorts of NAFLD patients, which limits the comprehensive understanding of NAFLD severity. We propose that integrating and analyzing these datasets with an unbiased gene-based profiling strategy will provide further insights into the molecular progression of NAFLD and the identification of

115 biomarkers associated with NAFLD severity. In the present study, we identified over
116 300 NAFLD biomarkers by integrating and analyzing RNA-seq data from 625 liver
117 samples, including their NAFLD activity scores (NAS) and fibrosis scores,
118 along with public proteomics data. We further validated these findings in two
119 independent NAFLD cohorts, demonstrating the potential of the QSOX1/IL1RAP ratio
120 as a non-invasive biomarker for diagnosing NAFLD and assessing its severity.
121

122 ## Materials and methods

123 **RNA-seq Data Analysis**

124 1. Data Collection

125 Genome-wide RNA-seq data of human NAFLD and associated healthy controls were
126 collected from the NCBI GEO (https://www.ncbi.nlm.nih.gov/gds, until May 2022).
127 Only datasets that provided detailed NAS and fibrosis scores were included for
128 further investigation.
129

130 2. Data Normalization

131 The SRA-formatted data were converted into FASTQ format using 'SraToolkit'
132 (sratoolkit.2.8.2-1-centos_linux64) (https://github.com/ncbi/sra-tools). Sequencing
133 reads were aligned to the hg19 UCSC RNA sequences Genome Reference Consortium
134 Human Build 37 (GRCh37) using 'bowtie2' (bowtie2-2.2.5)
135 (https://rnnh.github.io/bioinfo-notebook/docs/bowtie2.html). Only protein-coding
136 transcripts were considered, and Transcript Per Million (TPM) values were obtained
137 by transforming the mapped transcript reads using 'RSEM' (rsem-1.2.12)
138 (https://github.com/deweylab/RSEM). Then, TPM values were then subjected to
139 Trimmed Mean of M-values (TMM) normalization across all samples using 'metaseqR
140 ' (metaseqR 1.12.2) (14). The data from various sources involved in this study were
141 integrated and log1p-transformed, followed by batch correction using the
142 'removeBatchEffect' function in the R package 'limma' (limma 3.54.2)
143 (https://kasperdanielhansen.github.io/genbioconductor/html/limma.html) (15).

144 Subsequently, the data were expanded (10^x) for further analysis (**Figure 1A**).

145

146 3. RNA-seq Data Analysis and Database Construction

147 After normalization and batch correction, the RNA-seq data underwent Principal
148 Components Analysis (PCA) and unsupervised clustering using the R package 'Seurat'
149 (Seurat-4.3.0) (https://satijalab.org/seurat/articles/get_started.html). We utilized the
150 'LogNormalize' method for global-scaling normalization, which normalized the
151 feature expression measurements across different samples for each gene by the total
152 expression. The normalized values were multiplied by a scale factor (default:
153 10,000) and log1p-transformed. Subsequently, scaling was applied to the identified
154 variable features (default: 2,000). PCA was then performed on the scaled data, with a
155 default setting of computing and storing 50 Principal Components (PCs). To cluster
156 the genes, we employed modularity optimization techniques using a graph-based
157 clustering approach. The dimensions of reduction were set to 1:20, and
158 the resolution parameter was set to 2.3 (16).

159

160 To show the gene expression variation during the development of NAFLD associated
161 with both NAS and fibrosis scores, we generated an RNA-seq database using
162 'ShinyCell' (https://github.com/SGDDNB/ShinyCell). This database was deployed at
163 https://dreamapp.biomed.au.dk/NAFLD/.

164

165 **Proteomics Data Collection and Analysis**

166 The proteomics cohort dataset (PXD011839) includes 10 healthy controls, 10 NAFLD
167 patients with normal glucose tolerance (NAFLD_ngt), 10 NAFLD patients with type 2
168 diabetes (NAFLD_T2D), and 10 NAFLD patients with cirrhosis (17). We performed the
169 statistical analysis using R-4.3.0 on the dataset (EV1, tab4)
170 (https://www.ncbi.nlm.nih.gov/pmc/articles/PMC6396370/bin/MSB-15-e8793-s003.
171 xlsx). The NAFLD_ngt and NAFLD_T2D groups were merged into a single NAFLD group,
172 resulting in three groups: healthy controls, NAFLD, and cirrhosis.

173

174 Similar to RNA-seq analysis, we used 'Seurat' (Seurat-4.3.0) and employed the
175 'LogNormalize' method for global-scaling normalization. This method normalized the
176 feature expression measurements across different samples for each protein by the
177 total expression. The normalized values were multiplied by a scale factor (default:
178 10,000) and log1p-transformed. Subsequently, scaling was applied to the identified
179 variable features (default: 2,000). PCA was performed on the scaled data, with a total
180 of 39 Principal Components (PCs) computed and stored. Additionally, we calculated
181 the log fold-change of the average expression between two groups (avg_log2FC) by
182 comparing the health and NAFLD groups, as well as the NAFLD and cirrhosis groups.
183 By setting avg_log2FC > 0, we selected up- and down-regulated proteins associated
184 with increasing severity of NAFLD.
185
186 **Validation of QSOX1 and IL1RAP as Biomarkers in NAFLD**
187 1. Study Design
188 Our objective was to investigate whether *QSOX1* and *IL1RAP* gene expression levels,
189 as well as their encoded proteins, could predict the histological severity of NAFLD. To
190 address this issue, we investigated the plasma concentrations of QSOX1 and IL1RAP
191 in the proteomics data of healthy and NAFLD cohorts. Additionally, we conducted
192 enzyme-linked immunosorbent assay (ELISA) tests for plasma QSOX1/IL1RAP in a
193 cohort comprising healthy subjects and NAFLD patients recruited at Shenzhen
194 Traditional Chinese Medicine Hospital, China (SZTCMH).
195
196 2. Human Samples
197 A total of 28 ultrasound-proven adult NAFLD patients, including NAFLD_ngt and
198 NAFLD_T2D, and 14 healthy controls were enrolled from SZTCMH. Other diagnoses
199 and etiologies, such as excessive alcohol consumption, viral hepatitis, autoimmune
200 liver disease, and the use of steatogenic compounds, were excluded. Archived
201 plasma samples were collected between October and December 2022. Healthy
202 subjects and NAFLD patients were given informed consent according to the approved
203 clinical protocols of the Ethical Committee of SZTCMH. Clinical information, including

204 body mass index (BMI) and standard biochemistry (liver, kidney,
205 hematology) with metabolic profiling (glucose, insulin, lipids), was collected.
206 Fibroscan with controlled attenuation parameter (CAP) values was performed to
207 assess fibrosis and steatosis. Clinical information for the healthy controls and NAFLD
208 patients can be found in **Supplementary Table 4**.
209
210 For immunohistochemical staining (IHC), 12 fixed liver tissues were collected from
211 archived histological samples at SZTCMH between 2014 and 2023. These samples
212 were scored based on the NAS score (N0 to N8) and fibrosis score (F0 to F4) by two
213 pathologists (MMS and XWY). Six samples were from mild NAFLD patients (N0-4,
214 F0-2), and six were from severe NAFLD patients (N5-8, F3-4). The clinical study was
215 approved by the Ethical Committee of SZTCMH, and the approved clinical protocols
216 adhere to the Helsinki Declaration (No. K2022-174-01).
217
218 3. ELISA
219 Blind ELISA tests were conducted on the collected plasma samples. Randomly
220 assigned sample identifiers and positions were used to ensure blindness to the
221 clinical information and NAFLD stages. The levels of QSOX1 and IL1RAP were
222 measured using QSOX1 ELISA Kits (Catalog No. YJ145587, Lot No. 12/2022 from
223 Enzyme-linked Biotechnology, Shanghai, China) and IL1RAP ELISA Kits (Catalog No.
224 YJ130558, Lot No. 12/2022 from Enzyme-linked Biotechnology, Shanghai, China),
225 respectively. The measurements followed the manufacturer's instructions, and the
226 absorbance values were measured at 450nm. In order to ensure the reliability of the
227 ELISA Kits, a pre-experiment was conducted three times before the formal
228 experiment.
229
230 4. IHC
231 We examined the association of QSOX1 and IL1RAP with human NAFLD severity by
232 performing IHC on formalin-fixed and paraffin-embedded liver sections from 6 mild
233 NAFLD patients and 6 severe NAFLD patients. The 3 μm-thick paraffin sections were

234 deparaffinized and rehydrated with distilled water. Antigen retrieval was carried out
235 using pH 9.0 EDTA buffer, followed by 20 minutes of boiling and washing with 1X PBS.
236 Subsequently, the slides were blocked with 1% bovine serum albumin in 1X PBS for
237 15 minutes and then incubated overnight at 4℃ with QSOX1 (Rabbit anti-human,
238 Catalog No. Ab235444, Lot No. GR3386311-2 from Abcam) or IL1RAP (Rabbit
239 anti-human, Catalog No.35605, Lot No. 4926 from Sabbiotech) antibodies at a
240 concentration of 20 μg/ml. The following day, the slides were washed with 1X PBS
241 and incubated with Goat anti-rabbit IgG H&L (Catalog No. Ab205718, Lot No.
242 ab205718 from Abcam) for 15 minutes at room temperature, followed by another
243 wash with 1X PBS. The images were captured with a light microscope and 3DHISTECH
244 digital scanner (https://www.3dhistech.com/).
245
246 The IHC results were analyzed using the software tool '**ImagineJ (Fiji)'.** To prevent
247 potential bias, we randomly selected five locations of the same size from each
248 sample at 20x magnification using 3DHISTECH CaseViewer_2.4
249 (https://www.3dhistech.com/solutions/caseviewer/). Using 'ImagineJ', we applied
250 the 'Colour Deconvolution' tool with vectors=[H DAB], followed by selecting the
251 Colour_2 pictures and running '8-bit'. Standard thresholds were used (QSOX1:
252 setThreshold (60, 230), IL1RAP: setThreshold (94, 214)) (18, 19). The average
253 integrated density from the five sites was calculated and used as the integrated
254 density value for each sample, which was then subjected to statistical analysis.
255
256 5. Statistical analysis
257 The significance for all statistical tests was two-sided, with $P < 0.05$. All data analysis
258 was presented in the plots using R-4.3.0, and MedCalc was used to calculate the
259 AUROC, sensitivity, specificity, optimal cutoff value, and sample size.

Results

Overview of RNA-seq data and NAFLD patient cohorts

After applying stringent filtering criteria based on the availability of histological NAS and fibrosis scores, five datasets (including GSE115193, GSE134422, GSE135448, GSE160016, and GSE164441) were excluded from the analysis, while seven datasets (GSE105127, GSE107650, GSE126848, GSE130970, GSE135251, GSE162694, and GSE167523) were included. These datasets collectively comprise 81 healthy controls (N0F0) and 544 NAFLD patients. The severity of NAFLD patients was classified based on the NAS score (ranging from N1 to N8) and the fibrosis score (ranging from F0 to F4) using the scoring systems proposed by Brunt (20) and Kleiner (21), respectively (**Table 1**). A positive correlation was observed between NAS and fibrosis scores (Pearson R = 0.64, P = 4.94E-74, **Table 1**), indicating an association with NAFLD severity.

Normalization and Integration of RNA-seq Data

To address the issue of batch effects resulting from differences in sequencing technology and studies, we processed the integrated data as depicted in **Figure 1A**. Genes with low expression were filtered out, resulting in a total of 17,946 protein-coding genes. Principal component analysis (PCA) demonstrated that normalization effectively eliminated noticeable batch effects (**Figure 1B**). Moreover, neither the NAS nor fibrosis scores appeared to be the main factors contributing to sample separation (**Figure 1D, E**). Instead, the normalized RNA abundance (nCount) in each sample emerged as the key component influencing transcriptome profiles (**Figure 1C**).

Unsupervised Gene Clustering Identifies Clusters of Genes Associated with NAFLD Severity.

To identify genes associated with NAFLD severity, we utilized a previously developed unsupervised gene clustering method based on the similarity of gene expression

289 patterns across each sample (22). By setting a resolution of 2.3, we identified a total
290 of 38 gene clusters (**Supplementary Figure S1**). Notably, cluster 4, consisting of 1021
291 genes, consistently exhibited increased expression with higher NAS and fibrosis
292 scores (**Figure 2A, Supplementary Figure S2A**). Conversely, cluster 14, comprising
293 643 genes, showed decreased expression with increasing NAS and fibrosis scores
294 (**Figure 2B**, **Supplementary Figure S2B**).
295
296 To unveil the biological functions of these gene clusters, we performed Gene
297 Ontology (GO) analysis using the R package 'ClusterProfiler' (ClusterProfiler-4.8.0).
298 Specifically, we focused on cluster 4, which consisted of up-regulated genes. The GO
299 analysis revealed significant enrichment of genes involved in the fibrosis-related
300 process, such as extracellular matrix (ECM) organization (p.adjust = 9.77E-34),
301 extracellular structure organization (p.adjust = 9.77E-34), external encapsulating
302 structure organization (p.adjust = 1.09E-33), and cell-substrate adhesion (p.adjust =
303 3.35E-17). Notably, the expression of multiple genes involved in the ECM processes,
304 such as *COL5A3, FBLN5, SPINT2, COL1A1, COL1A2, COL3A1, COL4A1, COL4A4,*
305 *COL12A1, COL15A1*, and *COL16A1*, showed a gradual up-regulation during the
306 progression of NAFLD (**Figure 2A, Supplementary Figure S3**).
307
308 In contrast, cluster 14, which displayed a reverse correlation with NAS and fibrosis
309 scores, was significantly enriched in metabolic processes, indicating an association
310 between NAFLD progression and attenuated liver metabolism. The down-regulated
311 genes in this cluster were particularly enriched in processes such as organic acid
312 catabolic process (p.adjust = 2.57E-22), carboxylic acid catabolic process (p.adjust =
313 2.57E-22), small molecule catabolic process (p.adjust = 5.28E-22), alpha-amino acid
314 metabolic process (p.adjust = 6.03E-20), fatty acid metabolic process (p.adjust =
315 2.60E-10), and alcohol metabolic process (p.adjust = 1.35E-09). Notably, genes
316 encoding enzymes of the Cytochrome P450 superfamily, including *CYP1A2, CYP2C19,*
317 *CYP2J2, CYP2E1, CYP4A11, CYP4A22, CYP4F11, CYP2C8,* and *CYP3A4*, were
318 down-regulated with increasing NAFLD severity (**Figure 2B**, **Supplementary Figure**

319 **S4**). For a comprehensive list of all enriched GO terms for genes in cluster 4 and 14,
320 please refer to **Supplementary Table 1**.
321
322 In addition, we developed a NAFLD gene expression database (NAFLD-DB) to
323 facilitate the exploration and comparison of all identified protein-coding genes based
324 on NAFLD severity. The NAFLD-DB (https://dreamapp.biomed.au.dk/NAFLD/) was
325 constructed using the ShinyCell framework (23), which was specifically designed for
326 convenient exploration and sharing of single-cell transcriptome data.
327
328 **Identification of Candidate Diagnostic Biomarkers.**
329 We employed an additional complementary strategy to further refine our list of
330 candidate genes. In this approach, we first analyzed the plasma protein levels from a
331 NAFLD cohort in a proteomics dataset (PXD011839) (17). We selected proteins that
332 showed positive correlations with increasing NAFLD severity (avg_log2FC > 0) and
333 proteins that showed negative correlations. As a result, we identified 148
334 up-regulated proteins and 114 down-regulated proteins associated with increasing
335 NAFLD severity (**Figure 2C, D**).
336
337 The secretome, which consists of secreted proteins, has emerged as a valuable
338 resource for disease diagnostics (24-26). In our study, we aim to identify potential
339 diagnostic markers among the candidate genes by comparing our gene clusters with
340 the secretome database from the Human Protein Atlas (27). This cross-analysis
341 revealed a total of 349 genes encoding secreted proteins, with 249 genes showing
342 up-regulation and 100 genes showing down-regulation (**Figure 2E**). Notably, our
343 approach successfully identified a comprehensive list of previously known NAFLD
344 diagnostic and prognostic markers, including *ADAMTSL2* (28), *AEBP1* (29), and *BGN*
345 (30) (**Supplementary Table 2**), further validating the effectiveness of our approach.
346
347 Next, we intersected the protein-encoding genes of these proteins with the
348 secretome genes and the candidate genes generated from our RNA-seq analysis.

349 Through this cross-comparison, we identified 16 up-regulated secreting genes (*A2M,*
350 *C7, COL6A3, COLEC11, ENPP2, FBLN1, FBN1, FCGBP, IGFBP6, LCN2, LUM, MMP2,*
351 *PAPLN, PTGDS,* ***QSOX1****, VWF*) and 22 down-regulated secreting genes (*AZGP1, C1RL,*
352 *C4BPA, C6, C8B, CFHR3, CNDP1, F2, GC, HP, HPR,* ***IL1RAP****, ITIH1, ITIH2, ITIH4, KLKB1,*
353 *PON3, SERPINA10, SERPINC1, SERPING1, SMPDL3A, TTR*) associated with increasing
354 NAFLD severity in both the RNA-seq and proteomics data (**Supplementary Figure S5**).
355
356 **QSOX1 and IL1RAP are promising biomarkers for NAFLD severity**
357 To demonstrate the applicability of our NAFLD-DB and validate the association of
358 differential gene expression with increasing NAFLD severity, we selected two
359 representative genes, *QSOX1* and *IL1RAP,* which showed positive and negative
360 correlations with increasing NAFLD severity**.** We examined their expression levels in
361 comparison to patients with a NAS or fibrosis score of 0 (N0 or F0). The expression of
362 *QSOX1* was significantly correlated with the severity of NAFLD compared to N0 or F0
363 patients: N1-4 (p = 0.003), N5-8 (p = 1.9E-10), F1-2 (p = 0.001), F3-4 (p = 6.5E-8)
364 (**Figure 3A, B**). On the other hand, *IL1RAP* expression was significantly lower in
365 patients with increased NAFLD severity compared to N0 or F0: N1-4 (p = 1E-5), N5-8
366 (p = 4.7E-10), F1-2 (p = 0.00012), F3-4 (p = 0.00013) (**Figure 3C, D**).
367
368 Since *QSOX1* and *IL1RAP* exhibited opposite correlations with NAFLD severity, we
369 further explored whether the ratio of QSOX1/IL1RAP could better distinguish
370 between patient groups. Our results showed that compared to N0 or F0 patients, the
371 ratio of QSOX1 to IL1RAP mRNA levels showed even greater separation: N1-4 (p =
372 7.6E-8), N5-8 (5.9E-16), F1-2 (4.6E-6), F3-4 (6.8E-8) (**Figure 3E, F**). These findings
373 suggest that the QSOX1/IL1RAP ratio has the potential as a biomarker for diagnosing
374 NAFLD severity.
375
376 **Validation of Plasma QSOX1/IL1RAP Levels as Biomarkers for NAFLD Severity with**
377 **NAFLD Proteomics Cohort**
378 To further validate the potential of QSOX1 and IL1RAP as biomarkers for NAFLD

379 severity, we analyzed the plasma levels of QSOX1 and IL1RAP in a NAFLD proteomics
380 cohort (PXD011839) previously conducted by Niu L. and colleagues. This cohort
381 consisted of 10 healthy controls and 30 patients with NAFLD or NAFLD-induced
382 cirrhosis (17).
383
384 Consistent with our liver RNA profiling results in livers, the analysis of plasma
385 proteomics data from this independent NAFLD cohort showed a significant increase
386 in plasma QSOX1 levels in patients with NAFLD (Wilcoxon rank sum test, p = 0.021)
387 and cirrhosis (p = 0.049) compared to healthy controls (**Figure 4A**). Conversely,
388 IL1RAP levels were significantly reduced in patients with NAFLD (p = 5.8E-5) and
389 cirrhosis (p = 0.0011) (**Figure 4B**). Moreover, when considering the combined marker
390 of plasma QSOX1/IL1RAP ratio, it demonstrated even greater significance in
391 distinguishing NAFLD (p = 9.3E-6) and cirrhosis (p = 0.00013) patients from the
392 control group, compared to using QSOX1 or IL1RAP alone (**Figure 4C**).
393
394 To access the diagnostic sensitivity and specificity of QSOX1, IL1RAP, and their ratio
395 for NAFLD severity, we conducted ROC curve analysis using the 'MedCalc' tool (30).
396 The sample sizes for each comparison were evaluated and are listed in
397 **Supplementary Table 3**. The AUROC of the QSOX1/IL1RAP ratio for distinguishing
398 NAFLD patients from healthy controls was 0.95, with a cutoff value of 1.12. The
399 sensitivity was determined to be 90%, and the specificity was 100%. Notably, the
400 efficacy of the QSOX1/IL1RAP ratio was superior to that of IL1RAP alone
401 (AUROC=0.92) or QSOX1 alone (not significant). Similarly, when assessing the
402 differentiation between cirrhosis patients and healthy controls, the AUROC of the
403 QSOX1/IL1RAP ratio was 0.96, with a cutoff value of 1.12. The sensitivity was 90%,
404 and the specificity was 100%.
405
406 These results indicate that the QSOX1/IL1RAP ratio holds promise as a highly
407 effective biomarker for diagnosing NAFLD severity, surpassing the individual
408 biomarkers alone, and maintaining better sensitivity and specificity in distinguishing

409 NAFLD patients and cirrhosis patients from healthy individuals.

410

411 **Validation of QSOX1 and IL1RAP as biomarkers for NAFLD in another patient cohort**

412 To further validate the utility of QSOX1 and IL1RAP as biomarkers for NAFLD, we
413 conducted a validation study in healthy controls and NAFLD patients recruited from
414 the Department of Liver Disease of Shenzhen Traditional Chinese Medicine Hospital.
415 Plasma samples were collected from 14 healthy subjects and 28 newly diagnosed
416 NAFLD patients. Clinical information for the healthy controls and NAFLD patients can
417 be found in **Supplementary Table 4**.

418

419 We measured plasma levels of QSOX1 and IL1RAP using an enzyme-linked
420 immunosorbent assay (ELISA). Consistent with our previous findings, plasma levels of
421 QSOX1 (Wilcoxon rank sum test, $p = 0.043$), IL1RAP ($p = 0.035$), and the
422 QSOX1/IL1RAP ratio ($p = 0.00061$) were significantly different between NAFLD
423 patients and controls (**Figure 4D, E, F**).

424

425 To assess the diagnostic value of QSOX1 and IL1RAP as non-invasive biomarkers for
426 NAFLD by ELISA, we calculated the AUROC of the QSOX1/IL1RAP ratio in the ELISA
427 test to distinguish NAFLD patients from healthy controls. The QSOX1/IL1RAP ratio
428 exhibited an AUROC of 0.82. With a cutoff of 0.05, the sensitivity was 93%, and the
429 specificity was 57%. In comparison, the AUROC of QSOX1/IL1RAP ratio quantified by
430 ELISA showed less efficacy in distinguishing NAFLD patients from healthy controls
431 (**Supplementary Table 3**), which may be attributed to the sensitivity of protein
432 quantification methods and small sample size.

433

434 To further validate the association between QSOX1 and IL1RAP protein levels and
435 NAFLD severity, we assessed their levels in liver biopsies from mild and severe NAFLD
436 patients using IHC. Our results consistently demonstrated a significant correlation
437 between QSOX1 and IL1RAP levels and NAFLD severity (**Figure 5A**). Quantification of
438 QSOX1 and IL1RAP levels based on IHC confirmed that the QSOX1/IL1RAP ratio (p =

439 0.027) could distinguish the severe NAFLD group (n=6; NAS 5-8, fibrosis score 3-4)
440 from the mild NAFLD group (n=6; NAS 0-4, Fibrosis score 0-2) (**Figure 5B, C**).
441 Collectively, these findings suggest that the QSOX1/IL1RAP ratio holds promise as an
442 effective biomarker for the early diagnosis and prediction of NAFLD severity.

443 ## Discussion

444 This study is the first to integrate publicly available RNA-seq datasets from over 600
445 NAFLD patients with varying stages of disease severity, combined with proteomics
446 data analysis of publicly available datasets. The key findings suggest that the QSOX1
447 and IL1RAP, particularly the QSOX1/IL1RAP ratio hold promise as potential
448 biomarkers for NAFLD severity assessment. These results align with recent research
449 highlighting the importance of different transcriptional profiles specific to NAS and
450 fibrosis scores, offering valuable insights into the molecular mechanisms driving
451 disease progression from simple steatosis to inflammation and fibrosis (31, 32).
452

453 **The Advantages of Utilizing Integrated RNA-seq Data for Investigating NAFLD**
454 **Biomarkers**

455 Despite the growing availability of RNA-seq data in this field, many original studies
456 have been limited by small sample sizes and biased sample distribution, making it
457 challenging to accurately decipher transcriptional differences across various stages of
458 NAFLD(31-35). Several studies have attempted to identify diagnostic biomarkers and
459 potential drug targets. For instance, Brosch et al. conducted a positional analysis of
460 transcriptomes across three micro-dissected liver zones from 19 NAFLD patients (33).
461 Suppli et al. demonstrated that immunohistochemical markers offer greater
462 objectivity in distinguishing hepatocyte injury between NASH and NAFL (34). In the
463 pursuit of diagnostic genes and novel drug targets, Hoang et al. studied 6
464 histologically normal and 72 NAFLD patients, while Pantano et al. studied 31
465 histologically normal and 112 NAFLD patients. These studies revealed that specific
466 cells proportion and candidate gene signatures can accurately predict fibrosis stage
467 and disease progression (31, 32). Likewise, Govaere et al. observed the correlation
468 between gene expression and histology in a cohort of 10 controls and 206 NAFLD
469 patients (35). In contrast to the studies above that identified sets of potential
470 biomarker genes, Kozumi et al. validated thrombospondin 2 (THBS2) as a
471 non-invasive biomarker for NAFLD. They confirmed its potential in identifying the

472 disease stages among 98 NAFLD patients, and the serum levels of its encoded protein
473 TSP-2, measured by ELISA, showed an AUROC of 0.78 in the diagnosing of NASH
474 among 213 patients with biopsy-proven NAFLD (36). The major challenge of
475 combining and analyzing these diverse datasets lies in achieving homogeneous
476 processing, which requires substantial time and computational resources (37, 38). To
477 generate more robust and compelling results, we employed unbiased integration of
478 comprehensive NAFLD data to profile the liver transcriptome across a broad
479 spectrum of NAFLD severity in our study, incorporating all the aforementioned
480 samples.
481
482 **The Superiority of QSOX1 and IL1RAP as Potential Biomarkers of NAFLD**
483 The high prevalence and associated risks of NAFLD have driven global efforts to
484 identify improved diagnostic biomarkers. However, most existing biomarkers are
485 primarily suited for evaluating fibrosis (3, 39-41). The Fibrosis-4 (FIB-4) test,
486 commonly used in clinical practice, is sub-optimal for screening purposes, as it carries
487 the risks of both overdiagnosis and false negatives, particularly in patients at risk of
488 chronic liver disease (8). Although the patented ELF™ test was highly recommended
489 for ruling out advanced fibrosis, it comes with higher costs. Several steatosis scores,
490 such as the SteatoTest™ and the fatty liver index (FLI), have been proposed for
491 steatosis detection, but they do not provide substantial additional information
492 beyond routine clinical, laboratory, and imaging examinations conducted in
493 patients suspected of having NAFLD(8). Non-coding RNAs (ncRNAs), which exhibit
494 aberrant expression associated with NAFLD, have emerged as potential biomarkers
495 for NAFLD pathology, and circulating ncRNAs, including miR-122 and lncRNAs are
496 proposed as potential biomarkers for NAFLD severity and progression (42-48).
497 Despite the development of new biomarkers, there is still uncertainty surrounding
498 their predictive value, underscoring the urgent need to develop novel, cost-effective,
499 and efficient biomarkers with high sensitivity and specificity for NAFLD prediction
500 and monitoring (4, 49).
501

502 Previous studies have explored the relationship between QSOX1, IL1RAP, and NAFLD
503 or steatosis(12, 50). QSOX1 has been suggested as a potential diagnostic biomarker
504 for NAFLD, playing a significant role in lipid metabolism as an enzyme expressed in
505 various tissues, particularly in quiescent fibroblasts (33, 51, 52). IL1RAP is localized in
506 vesicles and cytosol, and it is secreted into the bloodstream. Notably, IL1RAP
507 expression at the RNA level was specifically detected in the liver and hepatocytes
508 (27). Hence, the combination of QSOX1 and IL1RAP as secretome genes and proteins
509 was selected as a potential biomarker combination.
510
511 The potential of QSOX1, IL1RAP, and their ratio as biomarkers for NAFLD was
512 demonstrated through the analysis of public RNA-seq and proteomics data, ELISA
513 tests conducted on patients' plasma, and IHC performed on fixed liver slides. These
514 findings suggest that QSOX1, IL1RAP, and their ratio hold promise as effective
515 biomarkers for NAFLD. Notably, the higher AUROC values for NAFLD diagnosis
516 achieved by QSOX1, IL1RAP, and their ratio highlight their efficacy as NAFLD
517 biomarkers.
518
519 **Limitation and Future Prospects.**
520 The current study possesses several strengths, including the integration and
521 processing of RNA-seq data from over 600 NAFLD patients with varying degrees of
522 NAFLD severity, as well as validation using proteomics data and samples from NAFLD
523 patients and controls. Furthermore, the well-established database with a
524 user-friendly interface could benefit the research community in exploring
525 differentially expressed genes in NAFLD at various stages. However, there are also
526 limitations to consider. For instance, some samples in the GSE126848 and GSE167523
527 datasets lacked individual NAS and fibrosis scores. To address this issue,
528 we standardized scores based on their categories in the original articles, and the
529 impact on the results was deemed negligible due to the provision of general stages
530 and unsupervised gene clustering. Machine learning, an essential tool for biomarker
531 validation and sample classification validation, should be employed to train large

532 cohorts of biopsy-proven NAFLD patients and healthy controls. However, this would
533 require an extended recruiting period(53) to determine the sensitivity and specificity
534 of the QSOX1/IL1RAP ratio for NAFLD diagnosis and staging.
535
536 Although newer technologies such as single-cell RNA sequencing (scRNA-seq) and
537 spatial sequencing have gained popularity, RNA-seq still serves as a valuable tool in
538 uncovering the pathogenesis of NAFLD (13). Computational analysis limitations make
539 it impractical for large cohort research, and single-cell suspension processing may
540 affect cell abundance and cell type representation, particularly in hepatic ballooning
541 cells in NAFLD (54). Single-nuclei RNA sequencing (snRNA-seq) captures cell
542 frequency more accurately than scRNA-seq but captures lower gene expression.
543 Spatial transcriptomics and proteomics have limitations for discovering invasive
544 biomarkers of NAFLD as they focus on small sampling areas (11). The combination of
545 all these biological tools holds potential for future research.
546
547 In conclusion, through a novel approach of unsupervised gene clustering performed
548 on integrated RNA-seq data, we have discovered a significant association between
549 QSOX1 and IL1RAP levels and NAFLD severity, with their ratio showing potential as a
550 non-invasive biomarker for diagnosing and assessing the severity of NAFLD.
551 Validation of our plasma-level findings in larger cohorts of liver biopsies is required,
552 but it holds promise as a new tool to diagnose NAFLD severity and reduce the need
553 for liver biopsies. Our approach may lead to the discovery of more NAFLD biomarkers,
554 and the ratios of other up-regulated and down-regulated genes associated with
555 increasing NAFLD severity also have the potential to be verified as potential
556 biomarkers.
557

558 **Abbreviations**

559 AUROC, area under the receiver operating characteristic; avg_log2FC, log fold-change
560 of the average expression between the two groups; BMI, body mass index; CK18,

561 circulating keratin 18 fragments; ECM, extracellular matrix; ELISA, enzyme-linked
562 immunosorbent assay; F, Fibrosis score; FIB-4, Fibrosis-4; GEO, Gene Expression
563 Omnibus; GO, Gene Ontology; GRCh37, Genome Reference Consortium Human Build
564 37; HCC, hepatocellular carcinoma; IHC, immunohistochemistry staining; IL1RAP,
565 Interleukin-1 receptor accessory protein; lg, log10; PCA, Principal components
566 analysis; QSOX1, Quiescin sulfhydryl oxidase 1; RNA-seq, RNA sequencing; N, NAS
567 score; NAFL, Non-alcoholic Fatty Liver; NAFLD, Non-alcoholic fatty liver disease;
568 NAFLD-DB, NAFLD gene expression database; NAFLD_ngt, NAFLD with normal
569 glucose tolerance; NAFLD_T2D, NAFLD with type 2 diabetes; NAS, NAFLD activity
570 scores; NASH, Non-alcoholic Steatohepatitis; ncRNAs, non-coding RNAs; scRNA-seq,
571 single-cell RNA sequencing; snRNA-seq, Single-nuclei RNA sequencing; SZTCMH,
572 Shenzhen Traditional Chinese Medicine Hospital, China; THBS2, thrombospondin 2;
573 TMM, Trimmed Mean of M-values; TPM, Transcript Per Million.
574

575 **Financial support**

576 This research was funded by the Shenzhen Science and Technology Project and
577 Sanming Project of Medicine in Shenzhen, China (grant nos. SZSM201612074,
578 JCYJ20180302173542393 and JCYJ20170817094901026).
579

580 **Authors' contributions**

581 YLL, HG, WFM and LL designed the study and interpreted the data. The analysis
582 strategy has been developed by LL and WFM. WFM, JRH, BQC, MLL, XZ, SMX and
583 MBK collected and assembled the data. WFM drafted the manuscript. WFM, JRH and
584 LC performed data analysis and/or interpretation. Technical support: YLL, LL, JRH, ZXZ,
585 MMS and XWY. Study participant inclusion: ZXZ, WFM, BQC, MLL, XZ, SMX, BLZ, QL,
586 QH, MQM. All authors reviewed and approved the final version of the manuscript.
587

588 **Data and code availability statement**

589 The data that support the findings of this study are available from the corresponding

author upon reasonable request.

Conflict of interest

Henning Grønbæk has received research grants from Abbvie, Intercept, ARLA Food for Health, ADS AIPHIA Development Services AG. Consulting Fees from Ipsen, NOVO, Pfizer. Lecturer for AstraZeneca and EISAI; and on Data Monitoring Committee at CAMURUS AB. All other authors have no conflicts of interest to declare.

Reference

1. Lazarus JV, Mark HE, Anstee QM, Arab JP, Batterham RL, Castera L, Cortez-Pinto H, et al. Advancing the global public health agenda for NAFLD: a consensus statement. Nat Rev Gastroenterol Hepatol 2022;19:60-78.
2. Riazi K, Azhari H, Charette JH, Underwood FE, King JA, Afshar EE, Swain MG, et al. The prevalence and incidence of NAFLD worldwide: a systematic review and meta-analysis. Lancet Gastroenterol Hepatol 2022;7:851-861.
3. Nassir F. NAFLD: Mechanisms, Treatments, and Biomarkers. Biomolecules 2022;12.
4. Vilar-Gomez E, Chalasani N. Non-invasive assessment of non-alcoholic fatty liver disease: Clinical prediction rules and blood-based biomarkers. J Hepatol 2018;68:305-315.
5. Kazankov K, Barrera F, Moller HJ, Rosso C, Bugianesi E, David E, Younes R, et al. The macrophage activation marker sCD163 is associated with morphological disease stages in patients with non-alcoholic fatty liver disease. Liver Int 2016;36:1549-1557.
6. Anstee QM, Castera L, Loomba R. Impact of non-invasive biomarkers on hepatology practice: Past, present and future. J Hepatol 2022;76:1362-1378.
7. Piazzolla VA, Mangia A. Noninvasive Diagnosis of NAFLD and NASH. Cells 2020;9.
8. European Association for the Study of the Liver. Electronic address eee, Clinical Practice Guideline P, Chair, representative EGB, Panel m. EASL Clinical Practice Guidelines on non-invasive tests for evaluation of liver disease severity and prognosis - 2021 update. J Hepatol 2021;75:659-689.
9. Barreby E, Chen P, Aouadi M. Macrophage functional diversity in NAFLD - more than inflammation. Nat Rev Endocrinol 2022;18:461-472.
10. Wang ZY, Keogh A, Waldt A, Cuttat R, Neri M, Zhu S, Schuierer S, et al. Single-cell and bulk transcriptomics of the liver reveals potential targets of NASH with fibrosis. Sci Rep 2021;11:19396.
11. Guilliams M, Bonnardel J, Haest B, Vanderborght B, Wagner C, Remmerie A, Bujko A, et al. Spatial proteogenomics reveals distinct and evolutionarily conserved hepatic macrophage niches. Cell 2022;185:379-396 e338.
12. Green CD, Dozmorov MG, Spiegel S. Analysis of Liver Responses to Non-alcoholic Steatohepatitis by mRNA-Sequencing. Methods Mol Biol 2022;2455:163-179.
13. Stark R, Grzelak M, Hadfield J. RNA sequencing: the teenage years. Nat Rev Genet 2019;20:631-656.

628 14. van den Berg RA, Hoefsloot HC, Westerhuis JA, Smilde AK, van der Werf MJ. Centering, scaling,
629 and transformations: improving the biological information content of metabolomics data. BMC
630 Genomics 2006;7:142.
631 15. Ritchie ME, Phipson B, Wu D, Hu Y, Law CW, Shi W, Smyth GK. limma powers differential
632 expression analyses for RNA-sequencing and microarray studies. Nucleic Acids Res 2015;43:e47.
633 16. Hao Y, Hao S, Andersen-Nissen E, Mauck WM, 3rd, Zheng S, Butler A, Lee MJ, et al. Integrated
634 analysis of multimodal single-cell data. Cell 2021;184:3573-3587 e3529.
635 17. Niu L, Geyer PE, Wewer Albrechtsen NJ, Gluud LL, Santos A, Doll S, Treit PV, et al. Plasma
636 proteome profiling discovers novel proteins associated with non-alcoholic fatty liver disease. Mol Syst
637 Biol 2019;15:e8793.
638 18. Schneider CA, Rasband WS, Eliceiri KW. NIH Image to ImageJ: 25 years of image analysis. Nat
639 Methods 2012;9:671-675.
640 19. Shu J, Dolman GE, Duan J, Qiu G, Ilyas M. Statistical colour models: an automated digital image
641 analysis method for quantification of histological biomarkers. Biomed Eng Online 2016;15:46.
642 20. Brunt EM, Janney CG, Di Bisceglie AM, Neuschwander-Tetri BA, Bacon BR. Nonalcoholic
643 steatohepatitis: a proposal for grading and staging the histological lesions. Am J Gastroenterol
644 1999;94:2467-2474.
645 21. Kleiner DE, Brunt EM, Van Natta M, Behling C, Contos MJ, Cummings OW, Ferrell LD, et al. Design
646 and validation of a histological scoring system for nonalcoholic fatty liver disease. Hepatology
647 2005;41:1313-1321.
648 22. Karlsson M, Sjostedt E, Oksvold P, Sivertsson A, Huang J, Alvez MB, Arif M, et al. Genome-wide
649 annotation of protein-coding genes in pig. BMC Biol 2022;20:25.
650 23. Ouyang JF, Kamaraj US, Cao EY, Rackham OJL. ShinyCell: Simple and sharable visualisation of
651 single-cell gene expression data. Bioinformatics 2021.
652 24. Liu Y, Ciotti GE, Eisinger-Mathason TSK. Hypoxia and the Tumor Secretome. Adv Exp Med Biol
653 2019;1136:57-69.
654 25. Crescenzi E, Leonardi A, Pacifico F. NGAL as a Potential Target in Tumor Microenvironment. Int J
655 Mol Sci 2021;22.
656 26. Zhou X, Zhang J, Lv W, Zhao C, Xia Y, Wu Y, Zhang Q. The pleiotropic roles of adipocyte secretome
657 in remodeling breast cancer. J Exp Clin Cancer Res 2022;41:203.
658 27. Uhlen M, Karlsson MJ, Hober A, Svensson AS, Scheffel J, Kotol D, Zhong W, et al. The human
659 secretome. Sci Signal 2019;12.
660 28. Corey KE, Pitts R, Lai M, Loureiro J, Masia R, Osganian SA, Gustafson JL, et al. ADAMTSL2 protein
661 and a soluble biomarker signature identify at-risk non-alcoholic steatohepatitis and fibrosis in adults
662 with NAFLD. J Hepatol 2022;76:25-33.
663 29. Gerhard GS, Hanson A, Wilhelmsen D, Piras IS, Still CD, Chu X, Petrick AT, et al. AEBP1 expression
664 increases with severity of fibrosis in NASH and is regulated by glucose, palmitate, and miR-372-3p.
665 PLoS One 2019;14:e0219764.
666 30. Cengiz M, Yilmaz G, Ozenirler S. Serum Biglycan as a Diagnostic Marker for Non-Alcoholic
667 Steatohepatitis and Liver Fibrosis. Clin Lab 2021;67.
668 31. Hoang SA, Oseini A, Feaver RE, Cole BK, Asgharpour A, Vincent R, Siddiqui M, et al. Gene
669 Expression Predicts Histological Severity and Reveals Distinct Molecular Profiles of Nonalcoholic Fatty
670 Liver Disease. Sci Rep 2019;9:12541.

671 32. Pantano L, Agyapong G, Shen Y, Zhuo Z, Fernandez-Albert F, Rust W, Knebel D, et al. Molecular
672 characterization and cell type composition deconvolution of fibrosis in NAFLD. Sci Rep 2021;11:18045.
673 33. Brosch M, Kattler K, Herrmann A, von Schonfels W, Nordstrom K, Seehofer D, Damm G, et al.
674 Epigenomic map of human liver reveals principles of zonated morphogenic and metabolic control. Nat
675 Commun 2018;9:4150.
676 34. Suppli MP, Rigbolt KTG, Veidal SS, Heeboll S, Eriksen PL, Demant M, Bagger JI, et al. Hepatic
677 transcriptome signatures in patients with varying degrees of nonalcoholic fatty liver disease compared
678 with healthy normal-weight individuals. Am J Physiol Gastrointest Liver Physiol 2019;316:G462-G472.
679 35. Govaere O, Cockell S, Tiniakos D, Queen R, Younes R, Vacca M, Alexander L, et al. Transcriptomic
680 profiling across the nonalcoholic fatty liver disease spectrum reveals gene signatures for
681 steatohepatitis and fibrosis. Sci Transl Med 2020;12.
682 36. Kozumi K, Kodama T, Murai H, Sakane S, Govaere O, Cockell S, Motooka D, et al. Transcriptomics
683 Identify Thrombospondin-2 as a Biomarker for NASH and Advanced Liver Fibrosis. Hepatology
684 2021;74:2452-2466.
685 37. Stupnikov A, McInerney CE, Savage KI, McIntosh SA, Emmert-Streib F, Kennedy R, Salto-Tellez M,
686 et al. Robustness of differential gene expression analysis of RNA-seq. Comput Struct Biotechnol J
687 2021;19:3470-3481.
688 38. Shakola F, Palejev D, Ivanov I. A Framework for Comparison and Assessment of Synthetic
689 RNA-Seq Data. Genes (Basel) 2022;13.
690 39. Tapper EB, Loomba R. Noninvasive imaging biomarker assessment of liver fibrosis by
691 elastography in NAFLD. Nat Rev Gastroenterol Hepatol 2018;15:274-282.
692 40. Masoodi M, Gastaldelli A, Hyotylainen T, Arretxe E, Alonso C, Gaggini M, Brosnan J, et al.
693 Metabolomics and lipidomics in NAFLD: biomarkers and non-invasive diagnostic tests. Nat Rev
694 Gastroenterol Hepatol 2021;18:835-856.
695 41. Wong VW, Adams LA, de Ledinghen V, Wong GL, Sookoian S. Noninvasive biomarkers in NAFLD
696 and NASH - current progress and future promise. Nat Rev Gastroenterol Hepatol 2018;15:461-478.
697 42. Panera N, Gnani D, Crudele A, Ceccarelli S, Nobili V, Alisi A. MicroRNAs as controlled systems and
698 controllers in non-alcoholic fatty liver disease. World J Gastroenterol 2014;20:15079-15086.
699 43. Fang Z, Dou G, Wang L. MicroRNAs in the Pathogenesis of Nonalcoholic Fatty Liver Disease. Int J
700 Biol Sci 2021;17:1851-1863.
701 44. Qian X, Zong W, Ma L, Yang Z, Chen W, Yan J, Xu J. MM-associated circular RNA downregulates
702 microRNA-19a through methylation to suppress proliferation of pancreatic adenocarcinoma cells.
703 Bioengineered 2022;13:9294-9300.
704 45. Jampoka K, Muangpaisarn P, Khongnomnan K, Treeprasertsuk S, Tangkijvanich P, Payungporn S.
705 Serum miR-29a and miR-122 as Potential Biomarkers for Non-Alcoholic Fatty Liver Disease (NAFLD).
706 Microrna 2018;7:215-222.
707 46. Akuta N, Kawamura Y, Suzuki F, Saitoh S, Arase Y, Fujiyama S, Sezaki H, et al. Analysis of
708 association between circulating miR-122 and histopathological features of nonalcoholic fatty liver
709 disease in patients free of hepatocellular carcinoma. BMC Gastroenterol 2016;16:141.
710 47. Wang W, Min L, Qiu X, Wu X, Liu C, Ma J, Zhang D, et al. Biological Function of Long Non-coding
711 RNA (LncRNA) Xist. Front Cell Dev Biol 2021;9:645647.
712 48. Atanasovska B, Rensen SS, Marsman G, Shiri-Sverdlov R, Withoff S, Kuipers F, Wijmenga C, et al.
713 Long Non-Coding RNAs Involved in Progression of Non-Alcoholic Fatty Liver Disease to Steatohepatitis.
714 Cells 2021;10.

715 49. Chee D, Ng CH, Chan KE, Huang DQ, Teng M, Muthiah M. The Past, Present, and Future of
716 Noninvasive Test in Chronic Liver Diseases. Med Clin North Am 2023;107:397-421.
717 50. Bozaoglu K, Attard C, Kulkarni H, Cummings N, Diego VP, Carless MA, Shields KA, et al. Plasma
718 levels of soluble interleukin 1 receptor accessory protein are reduced in obesity. J Clin Endocrinol
719 Metab 2014;99:3435-3443.
720 51. Gao R, Wang J, He X, Wang T, Zhou L, Ren Z, Yang J, et al. Comprehensive analysis of endoplasmic
721 reticulum-related and secretome gene expression profiles in the progression of non-alcoholic fatty
722 liver disease. Front Endocrinol (Lausanne) 2022;13:967016.
723 52. Reznik N, Fass D. Disulfide bond formation and redox regulation in the Golgi apparatus. FEBS Lett
724 2022;596:2859-2872.
725 53. Ledesma D, Symes S, Richards S. Advancements within Modern Machine Learning Methodology:
726 Impacts and Prospects in Biomarker Discovery. Curr Med Chem 2021;28:6512-6531.
727 54. Newman AM, Steen CB, Liu CL, Gentles AJ, Chaudhuri AA, Scherer F, Khodadoust MS, et al.
728 Determining cell type abundance and expression from bulk tissues with digital cytometry. Nat
729 Biotechnol 2019;37:773-782.
730

731 **Figure Legend**
732
733 **Figure 1. RNA sequencing data processing, integration, and analysis**
734 A. Illustration of data processing.
735 B. Principal component analysis (PCA) based on the origin of datasets.
736 C. PCA based on normalized RNA abundance (nCount).
737 D. PCA based on NAS score.
738 E. PCA based on fibrosis scores.
739
740
741 **Figure 2. Integrative transcriptome and proteomics analysis to identify NAFLD**
742 **biomarkers**
743 A. Heatmap presentation of 1021 up-regulated genes in cluster 4 associated with
744 increasing NAS scores.
745 B. Heatmap presentation of 643 down-regulated genes in cluster 14 associated with
746 increasing NAS scores.
747 C. Protein cluster of 148 up-regulated proteins associated with increasing NAFLD
748 severity in PXD011839.
749 D. Protein cluster of 114 down-regulated proteins associated with increasing NAFLD
750 severity in PXD011839.
751 E. (UP) Venn diagram showing 16 overlapping genes between up-regulated genes
752 identified by RNA-seq, up-regulated proteins in the plasma, and secreting proteins.
753 (DOWN) Venn diagram showing 22 overlapping genes between down-regulated
754 genes identified by RNA-seq, down-regulated proteins in the plasma, and secreting
755 proteins.
756
757 **Figure 3. Relationship between QSOX1/IL1RAP and NAS/fibrosis scores in**
758 **integrative RNA-seq data of the human liver.**
759 A. Box plot of QSOX1 gene expressions grouped by NAS scores (N0, N1-4, N5-8).
760 B. Box plot of QSOX1 gene expressions grouped by fibrosis stages (F0, F1-2, F3-4).
761 C. Box plot of IL1RAP gene expressions grouped by NAS scores (N0, N1-4, N5-8).
762 D. Box plot of IL1RAP gene expressions grouped by fibrosis stages (F0, F1-2, F3-4).
763 E. Box plot of QSOX1/IL1RAP gene expression ratio grouped by NAS scores (N0, N1-4,
764 N5-8).
765 F. Box plot of QSOX1/ IL1RAP gene expression ratio grouped by fibrosis stages (F0,
766 F1-2, F3-4).
767 Statistical testing was performed using the Wilcoxon rank sum test, with p-values
768 shown in the plot.
769
770 **Figure 4. Comparison of plasma protein QSOX1/IL1RAP between healthy**
771 **individuals and NAFLD at various stages.**
772 A-B. Box plots of plasma QSOX1 (A) and IL1RAP (B) protein levels in healthy
773 individuals, NAFLD patients, and cirrhosis patients quantified by mass spectrometry
774 in the NAFLD proteomics cohort.

C. Box plots of plasma QSOX1 and IL1RAP protein ratios in healthy controls, NAFLD patients, and cirrhosis patients quantified by mass spectrometry in the NAFLD proteomics cohort.

D-E. Box plots of plasma QSOX1 (D) and IL1RAP (E) protein levels in healthy controls and NAFLD groups (pg/ml) measured by ELISA.

F. Box plot of plasma QSOX1 and IL1RAP protein ratio.

Statistical testing was performed using the Wilcoxon rank sum test, with p-values shown in the plot.

Figure 5. Quantification of liver QSOX1 and IL1RAP levels in NAFLD patients by IHC.

A. Representative IHC images of QSOX1 and IL1RAP in liver biopsies from mild NAFLD patients (N0-4, F0-2) and severe NAFLD patients (N5-8, F3-4).

B. The integrated density of QSOX1 IHC. Box plots showing the log10 value.

C. The integrated density of IL1RAP IHC. Box plots showing the log10 value.

D. Box plot of QSOX1 and IL1RAP ratio of the integrated density quantified with IHC.

Statistical testing was performed using t-test, with p-values shown in the plot.

Table 1

Table 1: Characteristics of the populations studied

A total of 625 human liver samples of the full histological range from normal, NAFL, NASH to cirrhosis with the NAS (N) and fibrosis (F) scores provided in the database or original articles.

Sample distribution of NAS and FIB	F0	F1	F2	F3	F4	Age (yrs)	BMI (kg/m2)
						mean ± S.D.	mean ± S.D.
N0 (n)	81	1	1	-	1	46.4 ± 10.0	35.4 ± 9.1
N1 (n)	29	9	1	-	1	42.8 ± 12.7	36.1 ± 6.6
N2 (n)	27	10	1	-	1	51.9 ± 5.8	35.1 ± 6.0
N3 (n)	46	72	9	5	3	49.8 ± 9.4	34.6 ± 8.9
N4 (n)	30	19	20	15	3	49.6 ± 9.5	33.9 ± 4.6
N5 (n)	7	41	75	20	5	52.4 ± 11.7	32.5 ± 5.5
N6 (n)	1	18	17	18	3	53.2 ± 8.5	34.5 ± 5.6
N7 (n)	-	1	14	11	1	49.4 ± 9.8	36.3 ± 7.2
N8 (n)	-	-	2	4	2	54 ± 0.0	31.3± 0.0
Age (yrs) mean ± S.D.	46.6 ± 9.6	49.0 ± 10.6	53.2 ± 11.3	54.7 ± 6.0	54.8 ± 5.4		
BMI(kg/m2) mean ± S.D.	37.1± 8.3	32.4 ± 5.6	33.1 ± 7.0	32.5 ± 2.9	32.6 ± 2.2		
Gender n(male/female)	221(105/116)*	171 (108/63)*	140 (64/76)*	73 (35/38)*	20 (11/9)*		

Table 1. *The ratio of gender was estimated according to the gender ratio in the original articles. BMI, body mass index; N, NAS score; F, Fibrosis score.

Figure 1

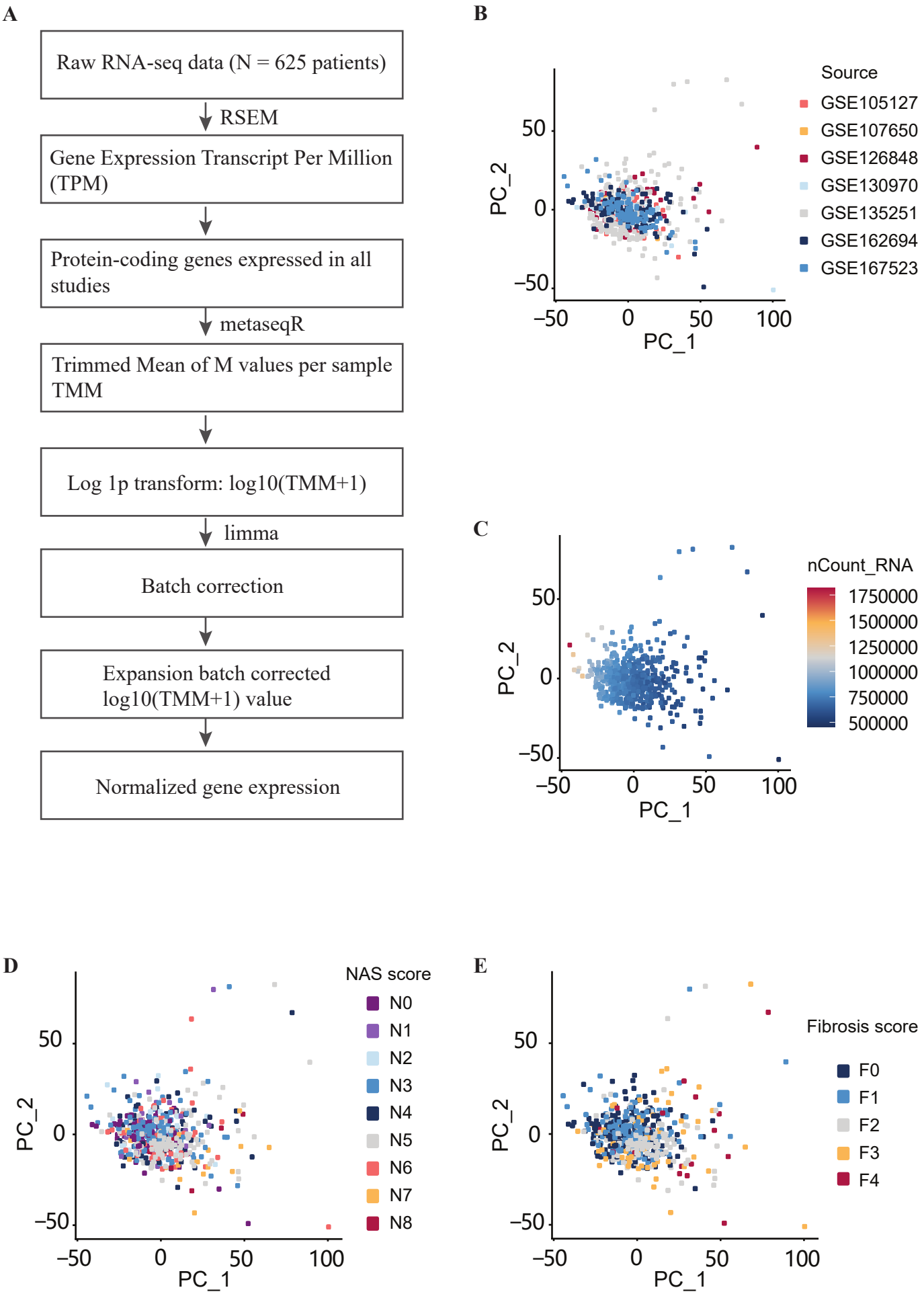
A
Raw RNA-seq data (N = 625 patients)
RSEM
Gene Expression Transcript Per Million (TPM)
Protein-coding genes expressed in all studies
metaseqR
Trimmed Mean of M values per sample TMM
Log 1p transform: log10(TMM+1)
limma
Batch correction
Expansion batch corrected log10(TMM+1) value
Normalized gene expression
B
Source
GSE105127
GSE107650
GSE126848
GSE130970
GSE135251
GSE162694
GSE167523
PC_2
PC_1
C
nCount_RNA
1750000
1500000
1250000
1000000
750000
500000
PC_2
PC_1
D
NAS score
N0
N1
N2
N3
N4
N5
N6
N7
N8
PC_2
PC_1
E
Fibrosis score
F0
F1
F2
F3
F4
PC_2
PC_1

Figure 2

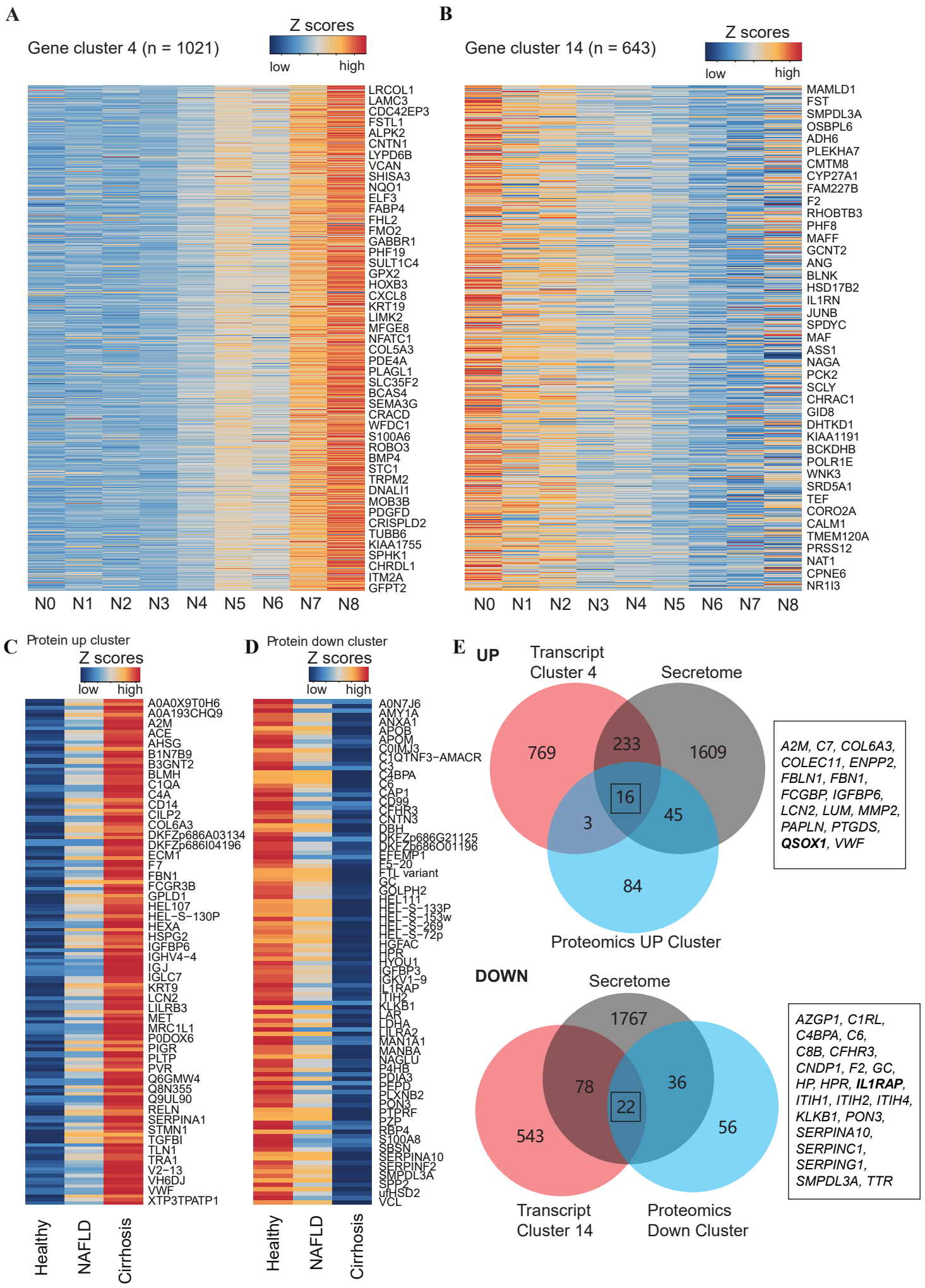
A
Gene cluster 4 (n = 1021)
Z scores
low
high
LRCOL1
LAMC3
CDC42EP3
FSTL1
ALPK2
CNTN1
LYPD6B
VCAN
SHISA3
NQO1
ELF3
FABP4
FHL2
FMO2
GABBR1
PHF19
SULT1C4
GPX2
HOXB3
CXCL8
KRT19
LIMK2
MFGE8
NFATC1
COL5A3
PDE4A
PLAGL1
SLC35F2
BCAS4
SEMA3G
CRACD
WFDC1
S100A6
ROBO3
BMP4
STC1
TRPM2
DNALI1
MOB3B
PDGFD
CRISPLD2
TUBB6
KIAA1755
SPHK1
CHRDL1
ITM2A
GFPT2
N0 N1 N2 N3 N4 N5 N6 N7 N8
B
Gene cluster 14 (n = 643)
Z scores
low
high
MAMLD1
FST
SMPDL3A
OSBPL6
ADH6
PLEKHA7
CMTM8
CYP27A1
FAM227B
F2
RHOBTB3
PHF8
MAFF
GCNT2
ANG
BLNK
HSD17B2
IL1RN
JUNB
SPDYC
MAF
ASS1
NAGA
PCK2
SCLY
CHRAC1
GID8
DHTKD1
KIAA1191
BCKDHB
POLR1E
WNK3
SRD5A1
TEF
CORO2A
CALM1
TMEM120A
PRSS12
NAT1
CPNE6
NR1I3
N0 N1 N2 N3 N4 N5 N6 N7 N8
C
Protein up cluster
Z scores
low
high
A0A0X9T0H6
A0A193CHQ9
A2M
ACE
AHSG
B1N7B9
B3GNT2
BLMH
C1QA
C4A
CD14
CILP2
COL6A3
DKFZp686A03134
DKFZp686I04196
ECM1
F7
FBN1
FCGR3B
GPLD1
HEL107
HEL-S-130P
HEXA
HSPG2
IGFBP6
IGHV4-4
IGJ
IGLC7
KRT9
LCN2
LILRB3
MET
MRC1L1
P0DOX6
PIGR
PLTP
PVR
Q6GMW4
Q8N355
Q9UL90
RELN
SERPINA1
STMN1
TGFBI
TLN1
TRA1
V2-13
VH6DJ
VWF
XTP3TPATP1
Healthy
NAFLD
Cirrhosis
D
Protein down cluster
Z scores
low
high
A0N7J6
AMY1A
ANXA1
APOB
APOM
C0IMJ3
C1QTNF3-AMACR
C3
C4BPA
C6
CAP1
CD99
CFHR3
CNTN3
DBH
DKFZp686G21125
DKFZp686O01196
EFEMP1
F5-20
FTL variant
GC
GOLPH2
HEL111
HEL-S-133P
HEL-S-153w
HEL-S-269
HEL-S-72p
HGFAC
HPR
HYOU1
IGFBP3
IGKV1-9
IL1RAP
ITIH2
KLKB1
LAR
LDHA
LILRA2
MAN1A1
MANBA
NAGLU
P4HB
PDIA3
PEPD
PLXNB2
PON3
PTPRF
PZP
RBP4
S100A8
SBSN
SERPINA10
SERPINF2
SMPDL3A
SPP2
ufHSD2
VCL
Healthy
NAFLD
Cirrhosis
E
UP
Transcript Cluster 4
Secretome
769
233
1609
16
3
45
84
Proteomics UP Cluster
A2M, C7, COL6A3, COLEC11, ENPP2, FBLN1, FBN1, FCGBP, IGFBP6, LCN2, LUM, MMP2, PAPLN, PTGDS, QSOX1, VWF
DOWN
Secretome
1767
78
36
22
543
56
Transcript Cluster 14
Proteomics Down Cluster
AZGP1, C1RL, C4BPA, C6, C8B, CFHR3, CNDP1, F2, GC, HP, HPR, IL1RAP, ITIH1, ITIH2, ITIH4, KLKB1, PON3, SERPINA10, SERPINC1, SERPING1, SMPDL3A, TTR

Figure 3

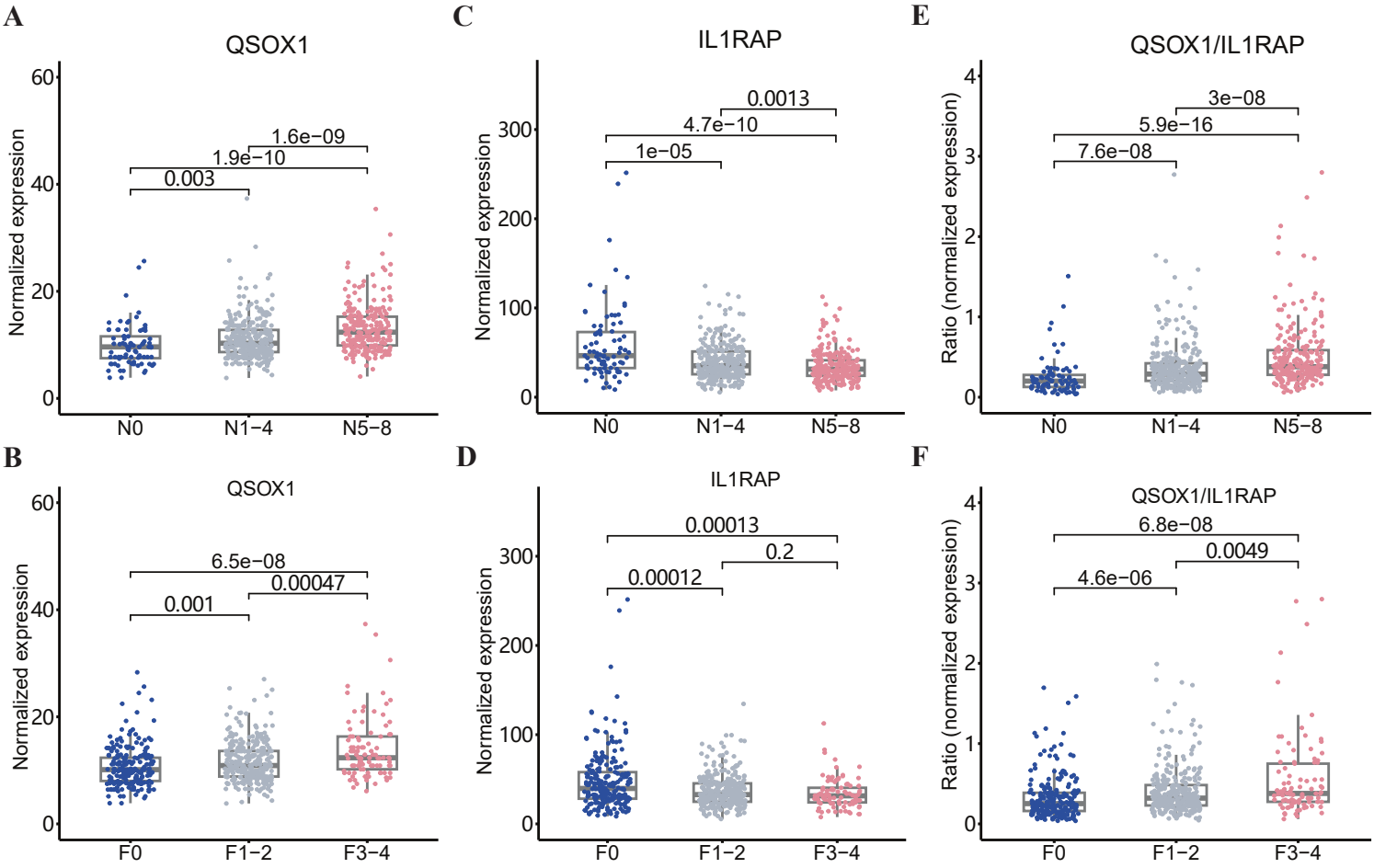
A
QSOX1
Normalized expression
0.003
1.9e−10
1.6e−09
N0
N1−4
N5−8
B
QSOX1
Normalized expression
0.001
6.5e−08
0.00047
F0
F1−2
F3−4
C
IL1RAP
Normalized expression
1e−05
4.7e−10
0.0013
N0
N1−4
N5−8
D
IL1RAP
Normalized expression
0.00012
0.00013
0.2
F0
F1−2
F3−4
E
QSOX1/IL1RAP
Ratio (normalized expression)
7.6e−08
5.9e−16
3e−08
N0
N1−4
N5−8
F
QSOX1/IL1RAP
Ratio (normalized expression)
4.6e−06
6.8e−08
0.0049
F0
F1−2
F3−4

Figure 4

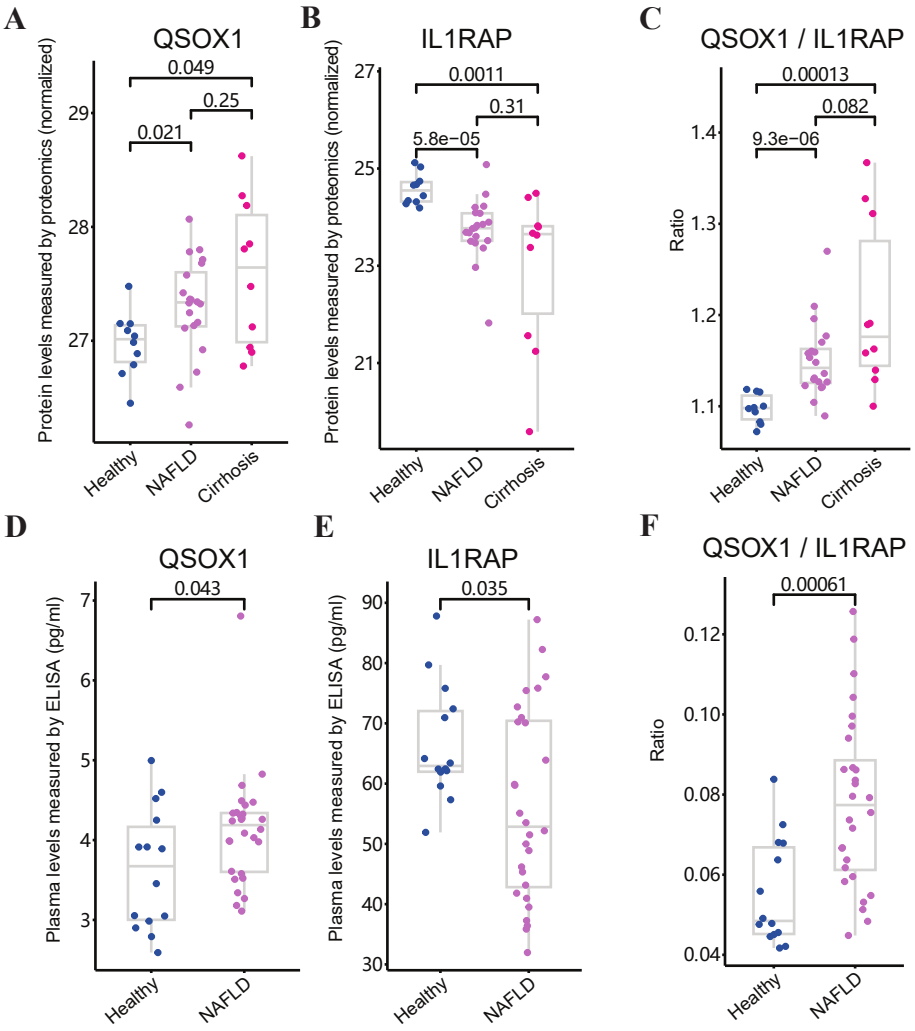
A
QSOX1
Protein levels measured by proteomics (normalized)
0.049
0.25
0.021
29
28
27
Healthy
NAFLD
Cirrhosis
B
IL1RAP
Protein levels measured by proteomics (normalized)
0.0011
0.31
5.8e−05
27
25
23
21
Healthy
NAFLD
Cirrhosis
C
QSOX1 / IL1RAP
Ratio
0.00013
0.082
9.3e−06
1.4
1.3
1.2
1.1
Healthy
NAFLD
Cirrhosis
D
QSOX1
Plasma levels measured by ELISA (pg/ml)
0.043
7
6
5
4
3
Healthy
NAFLD
E
IL1RAP
Plasma levels measured by ELISA (pg/ml)
0.035
90
80
70
60
50
40
30
Healthy
NAFLD
F
QSOX1 / IL1RAP
Ratio
0.00061
0.12
0.10
0.08
0.06
0.04
Healthy
NAFLD

Figure 5

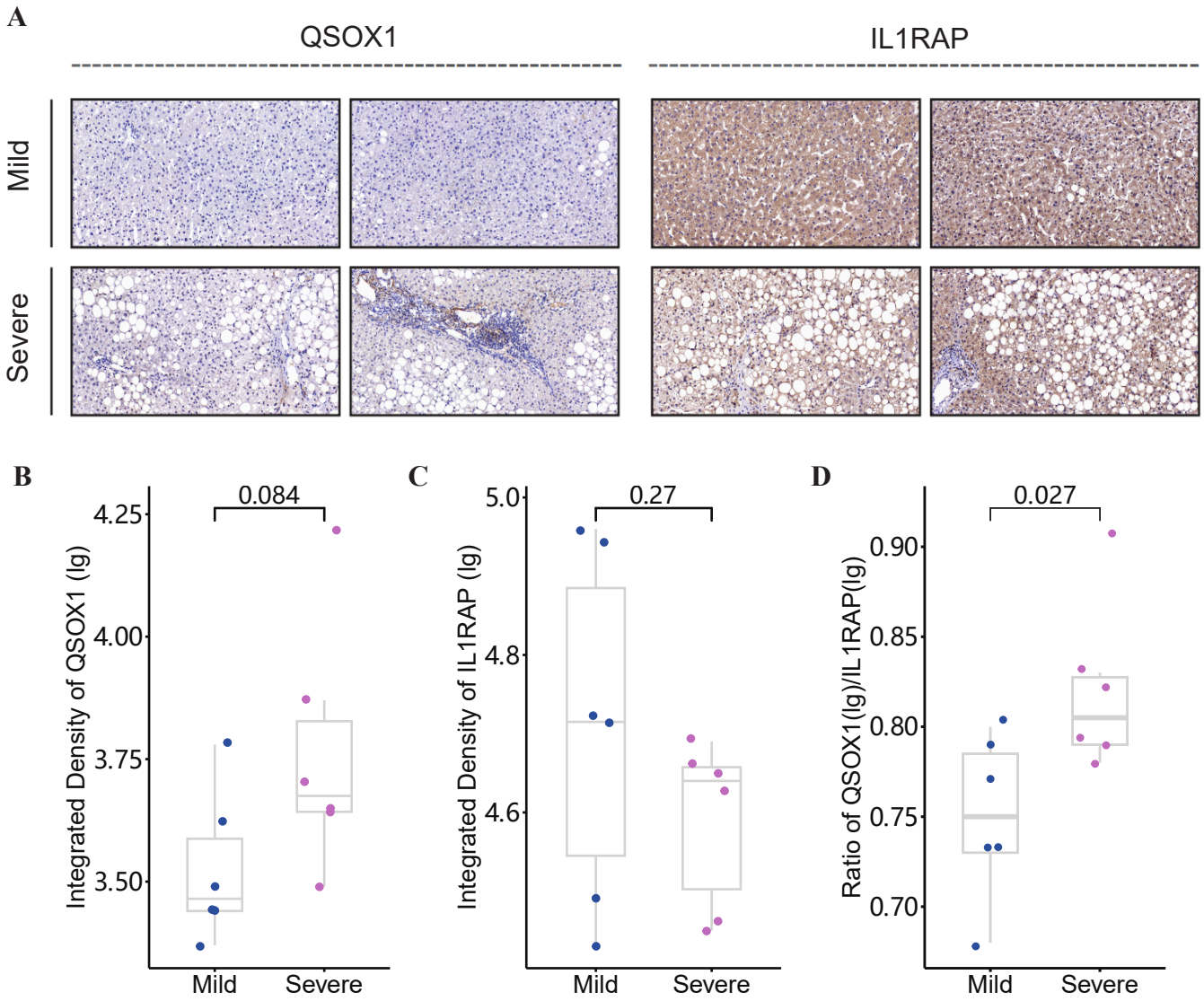
A
QSOX1
IL1RAP
Mild
Severe
B
0.084
Integrated Density of QSOX1 (Ig)
4.25
4.00
3.75
3.50
Mild
Severe
C
0.27
Integrated Density of IL1RAP (Ig)
5.0
4.8
4.6
Mild
Severe
D
0.027
Ratio of QSOX1(Ig)/IL1RAP(Ig)
0.90
0.85
0.80
0.75
0.70
Mild
Severe